Journal of Solid State Chemistry 183 (2010) 1380–1387

Contents lists available at ScienceDirect

Journal of Solid State Chemistry

journal homepage: www.elsevier.com/locate/jssc

Dielectric properties of some $MM'O_4$ and $MTiM'O_6$ (M=Cr, Fe, Ga; M'=Nb, Ta, Sb) rutile-type oxides

Rohini Mani [a], S.N. Achary [b], Keka R. Chakraborty [c], S.K. Deshpande [d], Joby E. Joy [a], Abanti Nag [a], J. Gopalakrishnan [a,*], A.K. Tyagi [b,*]

[a] Solid State and Structural Chemistry Unit, Indian Institute of Science, Bangalore 560 012, India
[b] Chemistry Division, Bhabha Atomic Research Centre, Mumbai 400085, India
[c] Solid State Physics Division, Bhabha Atomic Research Centre, Mumbai 400085, India
[d] UGC-DAE Consortium for Scientific Research, Bhabha Atomic Research Centre, Mumbai 400085, India

ARTICLE INFO

Article history:
Received 18 November 2009
Received in revised form
10 April 2010
Accepted 14 April 2010
Available online 18 April 2010

Keywords:
Rutile oxides
$MM'O4$
$MTiM'O_6$
Dielectric
Relaxor ferroelectric

ABSTRACT

We describe an investigation of the structure and dielectric properties of $MM'O_4$ and $MTiM'O_6$ rutile-type oxides for M=Cr, Fe, Ga and M'=Nb, Ta and Sb. All the oxides adopt a disordered rutile structure ($P4_2/mnm$) at ambient temperature. A partial ordered trirutile-type structure is confirmed for $FeTaO_4$ from the low temperature (17 K) neutron diffraction studies. While both the $MM'O_4$ oxides ($CrTaO_4$ and $FeTaO_4$) investigated show a normal dielectric property $MTiM'O_6$ oxides for M=Fe, Cr and M'=Nb/Ta/Sb display a distinct relaxor/relaxor-like response. Significantly the corresponding gallium analogs, $GaTiNbO_6$ and $GaTiTaO_6$, do not show a relaxor response at $T<500$ K.

1. Introduction

Rutile (TiO_2) is a well-known inorganic structure that has been investigated for several applications such as photocatalyst for splitting water into hydrogen and oxygen [1] and abatement of organic pollution [2]. Rutile (TiO_2) is also known for its incipient ferroelectric property because of its large static dielectric permittivity that shows strong frequency dependence and the associated soft (A_{2u}) mode behavior [3]. Rutile represents a generic inorganic structure (Fig. 1) adopted by several metal oxides of MO_2, $MM'O_4$ and MM'_2O_6 stoichiometries [4].

We have recently reported [5] a strong relaxor ferroelectric behavior for the rutile based oxide, $FeTiTaO_6$, that is comparable to the best relaxor materials such as $Pb_3MgNb_2O_9$ and $Pb_3ZnNb_2O_9$. The corresponding Cr-analog $CrTiTaO_6$ also showed a weak relaxor effect [5]. Considering the significance of this work for the development of lead-free relaxors [6,7], we extend our investigation of the dielectric properties to several other $MM'O_4$ and $MTiM'O_6$, for M=Fe, Cr, Ga and M'=Nb, Ta, Sb rutile-type oxides with a view to understand the origin of ferroelectric response in rutile based oxides in general. The salient results of these studies are reported in this paper.

2. Experimental

The $MM'O_4$-type $FeTaO_4$ and $CrTAO_4$ and $MTiM'O_6$-type $FeTiNbO_6$, $FeTiSbO_6$, $CrTiSbO_6$, $CrTiNbO_6$, $GaTiNbO_6$ and $GaTiTaO_6$ were synthesized by conventional solid state reaction of appropriate starting materials ($FeC_2O_4\cdot 2H_2O/Cr_2O_3/Ga_2O_3$, $Nb_2O_5/Ta_2O_5/Sb_2O_3$) at elevated temperatures (up to 1300 °C) in air with several intermittent grindings. Powder X-ray diffraction (XRD) patterns of the final products were recorded at ambient temperature (298 K) with a PANalytical X'Pert Diffractometer operated at 40 KV and 30 mA using Ni filtered Cu $K\alpha$ radiation. Neutron diffraction data of the powder samples $MTaO_4$ (M=Cr, Fe) were recorded at the Dhruva reactor, BARC Mumbai, at the beam port T1013. The beam port is equipped with a five PSD powder diffractometer. Data were recorded in the 2θ range of 5–138° with a step width of 0.05°, at 300 and 17 K for $FeTaO_4$ and at 300 and 12 K for $CrTaO_4$. This diffraction data were collected employing neutrons of wavelength 1.249 Å. Lattice parameters were obtained by least squares refinement of powder XRD data by the program PROSZKI [8]. Powder XRD patterns were also simulated by the program POWDERCELL [9] and refined by the

* Corresponding authors.
E-mail addresses: gopal@sscu.iisc.ernet.in (J. Gopalakrishnan), aktyagi@barc.gov.in (A.K. Tyagi).

0022-4596/$ - see front matter © 2010 Elsevier Inc. All rights reserved.
doi:10.1016/j.jssc.2010.04.022

program GSAS [10] and Fullprof 2 K [11]. The structural parameters obtained from the refinement of the studied materials are summarized in Table 1.

Temperature-dependent dielectric measurements were carried out using the Novocontrol Alpha impedance analyzer equipped with a Quatro nitrogen gas cryosystem. Samples in the form of sintered cylindrical pellets (about 8 mm in diameter and 2 mm thick) were sandwiched between two gold plated electrodes in the Novocontrol BDS1200 sample cell. Silver paint was coated on the sample surfaces for making proper electrical contact. The measurements were done over a frequency range of 100 Hz–10 MHz at several temperatures between 300 and 625 K.

3. Results and discussion

3.1. Structure

The observed XRD patterns of various studied compositions show typical reflections similar to those of rutile-type TiO_2. Further characterizations of the prepared compositions were carried out by Rietveld refinement of the corresponding XRD patterns using structural parameters of rutile as initial model. The final Rietveld refinement plots for representative compositions, namely, $CrTaO_4$ and $FeTiNbO_6$ are shown in Figs. 2 and 3,

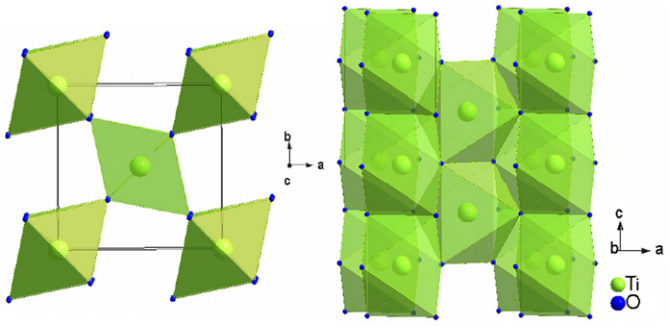

Fig. 1. Structure of rutile as viewed along the (a) *c*-axis and (b) *b*-axis.

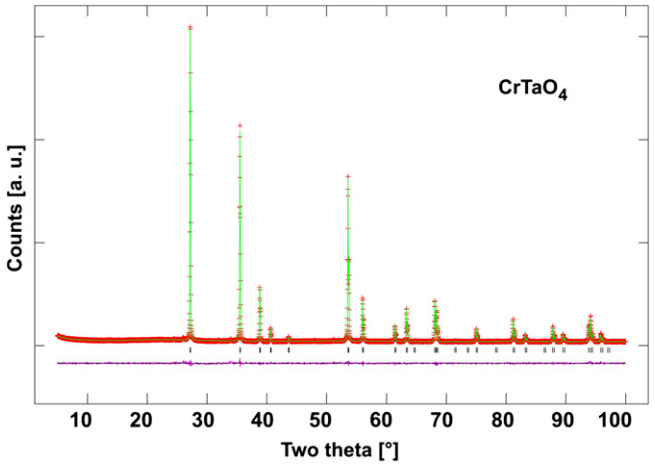

Fig. 2. Rietveld refinement of the structure of $CrTaO_4$ from XRD data.

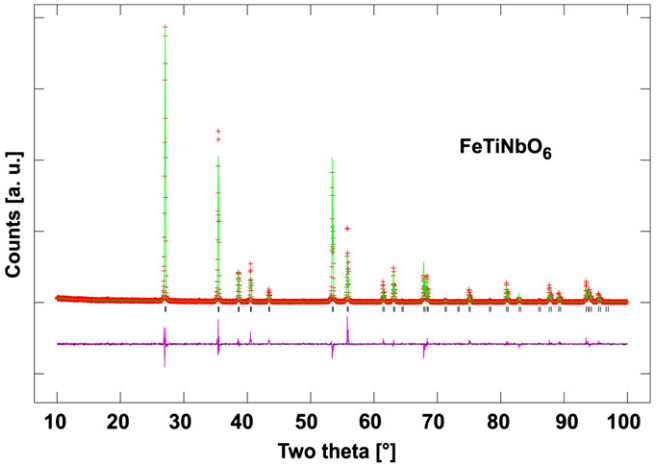

Fig. 3. Rietveld refinement of the structure of $FeTiNbO_6$ from XRD data.

Table 1
Structural parameters for $MM'O_4$ and $MTiM'O_6$ rutile-type oxides.

Oxides	*a* (Å)	*c* (Å)	*c*/*a*	*V* (Å^3)	*x*[a]	U_{iso} (Å^2)[b] (O)	U_{iso} (Å^2)[b] (M)	R_p, R_{wp},x^2 $R_F{}^2$	*d* (M–O) (Å)	Av (M–O) (Å)
$FeTaO_4$	4.6809(1)	3.0501(1)	0.6516	66.83(1)	0.2997(6)	–	–	0.0497, 0.0635, 1.437, 0.0646	1.984(4) × 2 2.021(3) × 4	2.009
$CrTaO_4$	4.6435(1)	3.0200(1)	0.6504	65.12(1)	0.3019(4)	1.29(7)	1.60(2)	0.0351, 0.0484, 1.500, 0.0250	1.983(3) × 2 1.993(2) × 4	1.990
$FeTiSbO_6$	4.6232(2)	3.0364(2)	0.6568	64.90(1)	0.2995(5)	0.94(10)	0.75(3)	0.0477 0.0299, 5.704, 0.0513	1.958(3) × 2 2.006(2) × 4	1.990
$CrTiNbO_6$	4.6297(2)	2.9960(1)	0.6471	64.22(1)	0.3032(4)	1.42(1)	2.24(1)	0.0480, 0.0696, 3.935, 0.0494	1.985(2) × 2 1.976(2) × 4	1.979
$GaTiTaO_6$	4.6259(1)	3.0046(1)	0.6495	64.29(1)	0.3027(5)	1.80(2)	1.64(2)	0.0522,0.0726, 3.913 0.0407	1.980(3) × 2 1.981(2) × 4	1.981
$FeTiTaO_6$[c]	4.655(4)	3.021(2)	0.6490	65.45	0.3034	–	–	–	1.997 × 2 1.989 × 4	1.992
$CrTiTaO_6$[c]	4.633(5)	3.003(4)	0.6482	64.44	0.3011	–	–	–	1.988 × 4 1.972 × 2	1.983
TiO_2[d]	4.593(2)	2.959(1)	0.6442	62.42	0.3060	–	–	–	1.943 × 4 1.988 × 2	1.958
$GaTiNbO_6$	4.6303(2)	3.0012(1)	0.6482	64.35(1)	0.297(1)	3.8(2)	1.4(1)	0.1554, 0.2185, 4.744, 0.1597	1.945(7) × 2 2.005(5) × 4	1.983
$FeTiNbO_6$	4.6557(2)	3.0154(1)	0.6477	65.36(1)	0.2947(7)	3.1(1)	1.9(1)	0.1425, 0.1857, 2.863, 0.1556	1.938(4) × 2 2.026(4) × 4	1.997

[a] Variable position parameter of oxygen in rutile ($P4_2/mnm$) structure. (Position of atoms M: 2*a* (0 0 0); O: 4*f* (*x x* 0)).
[b] × 100.
[c] Data taken from Ref. [5].
[d] Data taken from ICSD 34372.

respectively. The final Rietveld refinement plots of all other compositions are shown in Supplementary materials (SI-SVI). All the XRD patterns could be refined very well with the rutile based model as observed from the acceptable residuals from the refinements (Table 1).

The XRD patterns observed for $FeTiNbO_6$ and $GaTiNbO_6$ show appreciable difference compared to the corresponding pattern calculated by model based on rutile-type structure. This is also evident from the higher values of residuals compared to all other cases (Table 1). The observed powder X-ray profiles could not be modeled using preferred orientation functions, even with more than one orientation vectors. The higher values of residuals in the case of $FeTiNbO_6$ and $GaTiNbO_6$ might be due to the structural distortions, which are reflected in the intensity variations and abnormality of profiles in some peaks (Fig. 3 and Supplementary materials). It can also be mentioned here that $FeNbO_4$ is known to have different crystallographic modification depending on preparation and conditions of measurements [4,12]. Similarly, the $GaNbO_6$ preferentially crystallizes in a monoclinic lattice like $AlNbO_4$ [13]. Attempts to refine these two XRD pattern with the model based on ordered structures of $FeNbO_4$ or $GaNbO_4$ were also not successful. Thus it has been assumed that the real structure of the $FeTiNbO_6$ and $GaTiNbO_6$ may be different from rutile-type structure even though it broadly agrees with the tetragonal ($P4_2/mnm$: rutile type) structure. Earlier diffraction studies by Blasse [14] for a series of $MTiM'O_6$ compositions indicate that $MTiSbO_6$ for M=Sc, Cr, Ga and Al; $MTiTaO_6$ for M=Sc, Cr, Ga and Al; and $CrTiNbO_6$ have undoubtedly form rutile-type structures. However, the diffraction data reported for $GaTiNbO_6$ indicates the formation of rutile-type phase in addition to an unidentified phase [14]. In the present study though no additional reflections are observed, the intensity mismatch in the observed and calculated diffraction pattern indicates a distorted or partially ordered phase in $FeTiNbO_6$ and $GaTiNbO_6$ compositions. Hence further study is required to draw more conclusions about their crystal structure of $FeTiNbO_6$ and $GaTiNbO_6$. For the present purpose we conclude that all the studied compositions have rutile-type structure with or without any significant distortion. Thus it has been generalized that M/M' and M/Ti/M' atoms are disordered at the *2a* sites in a broader sense.

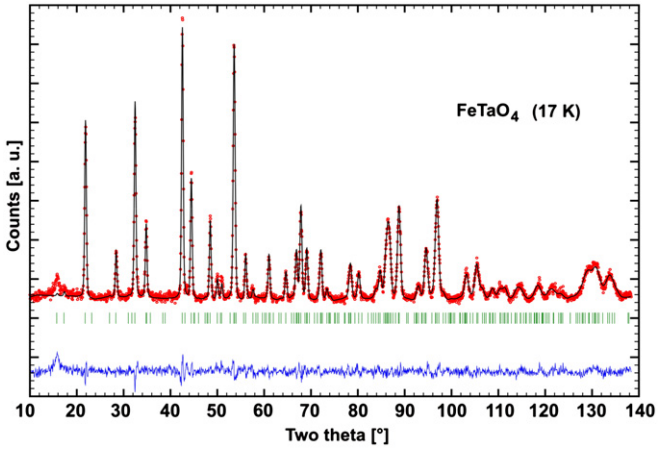

Fig. 4. Rietveld refinement of the structure of $FeTaO_4$ from ND data collected at 17 K, based on the trirutile ($P4_2/mnm$) model.

In order to compare the structural nature of $CrTaO_4$ and $FeTaO_4$, neutron diffraction data at low temperature were analyzed. The observed low temperature neutron diffraction data of $CrTaO_4$ revealed a similar disordered rutile structure. However, the low temperature neutron diffraction pattern for $FeTaO_4$ shows several weak reflections at $2\theta \sim 15.7°$, 17.2°, 26.9°, etc. Structural differences between $CrNbO_4$ and $FeTaO_4$ have been earlier reported by Christensen et al. [15] from a variable temperature neutron diffraction studies. Considering that ordered variables of the rutile structure are known for both $MM'O_4$ and MM'_2O_6 oxides {e.g. $CoReO_4$ (*Cmmm*) [16], $AlWO_4$ (*C2/m*) [17], $CuUO_4$ ($P2_1/n$) [18]; $FeTa_2O_6$ ($P4_2/mnm$) [19] and $LiNbWO_6$ (*P*-42$_1m$) [20]}, we examined the possibility of ordered structures for the oxides by low temperature neutron diffraction in selected cases. Among the oxides examined, we found from ND data at 17 K $FeTaO_4$ adopted a partially ordered trirutile structure (Fig. 4 and Table 2). A disordered rutile type and a partially disordered trirutile-type structures have been concluded for $CrNbO_4$ and $FeNbO_4$, respectively.

Further we examined the distribution of the metal ions in 2*a* and 4*e* sites of space group $P4_2/mnm$ by considering a distributed structural model as $[Fe_{0.5+x}Ta_{0.5-x}]_{2a}[Fe_{0.5-x/2}Ta_{0.5+x/2}]_{4e}[O]_{4f}[O]_{8j}$. In normal trirutile compositions ($FeTa_2O_6$) usually the reflections appreciable while the presence of partial disorder of cation in the 4*e* sites leads to weak feature. The occupation of metal ions varied in steps and concluded that the $[Fe]_{2a}[Fe_{0.25}Ta_{0.75}]_{4e}[O]_{4f}[O]_{8j}$ composition show a better match in observed and calculated diffraction data. The final Rietveld refinement plots of the low temperature powder neutron diffraction data of $FeTaO_4$ are shown in Fig. 4. Refined structural parameters for trirutile-type $FeTaO_4$ are given in Table 2. Christensen et al. [15] also have reported a similar result for this oxide with the cation distribution $[Fe]_{2a}[Fe_{0.50}Ta_{1.50}]_{4e}O_6$ at 8 K. This indicates a preferential segregation of Fe atoms at the 2*a* sites. However, the present structural refinement as well as the diffraction data reported earlier show a significant discrepancy in the intensity and width of the low angle peak (0 0 2 plane of trirutile lattice). With a constraint of nominal composition, any sorts of cation distribution alone could not explain the intensity of the 0 0 2 reflection (see Fig S-VII Supplementary information). Variable temperature neutron diffraction data reported earlier [15,21] for such materials indicate that the intensity and width of the 0 0 2 peak increases at lower

Table 2
Refined crystallographic data for $FeTaO_4$ from ND data at 17 K for the trirutile model.

Atom	Site	*x*	y	z	B_{iso} (Å^2)	Occupancy
Fe1	2*a*	0	0	0	0.34(15)	1
Fe2/Ta2	4*e*	0	0	0.3353(11)	0.35(10)	0.25/0.75
O1	4*f*	0.2973(15)	0.2973(15)	0	0.34(5)	1
O2	8*j*	0.3053(8)	0.3053(8)	0.3475(9)	0.36(3)	1

Space group: $P4_2/mnm$, a=4.6734(2) Å, c=9.1304(5) Å, V=199.41(2) Å^2
Reliability factors: R_p=5.09, R_{wp}=6.63, R_B=5.86, R_F^2=4.92, χ^2=2.75
Bond lengths (Å): Fe(1)–O(1)=1.965(7)(× 2), Fe(1)–O(2)=1.965(6)(× 4),
Fe(2)/Ta(2)–O(1)=2.014(9)(× 2), Fe(2)/Ta(2)–O(2)=2.018(4)(× 2)
Fe(2)/Ta(2)–O(2)=2.035(10)(× 2)
Bond valence sums: Fe(1)=3.4, Fe(2)/Ta(2)=4.2

temperature. The short range magnetic ordering Fe^{3+} of the 2*a* site has been attributed to such increasing intensity of 002 reflection. Thus we expect that such short range magnetic ordering may be the reason for the difference in the intensity of the low angle peaks of the present low temperature neutron diffraction data of $FeTaO_4$. On the other hand, $CrTaO_4$ showed a completely disordered rutile structure even at 12 K. The present observations for $CrTaO_4$ and $FeTaO_4$ are in close agreement with that reported earlier by Christensen et al. [15]. Similar neutron diffraction studies on $FeTiTaO_6$ and $CrTiTaO_6$ also showed a disordered rutile structure down to 12 K [5].

In summary of the structural studies we conclude that at ambient temperature all the studied compositions preferably retain the disordered rutile-type structure. In Table 1, we also included the structural data for $FeTiTaO_6$ and $CrTiTaO_6$ from our earlier work [5], together with the data for rutile TiO_2 from the literature for a ready comparison. In all the compositions, a distorted octahedral environment around *M*/*M*′ and *M*/Ti'*M* is observed. The typical *M*/*M*′–O or *M*/Ti/*M*′–O bond lengths are included in Table 1. The average bond lengths are larger compared to that of TiO_2 as expected from the ionic radii differences. However, the axial ratios (*c*/*a*) for the studied compositions are almost similar to that of TiO_2 (rutile).

3.2. Dielectric properties

The complex dielectric permittivity $\varepsilon^*(\omega)$ was extracted from the impedance data using [22]

$$\varepsilon^*(\omega) = [(A/l)i\omega\varepsilon_0 Z^*(\omega)]^{-1} \quad (1)$$

where $\omega = 2\pi f$ is the angular frequency, f the frequency of applied AC voltage, Z^* the complex impedance, ε_0 the permittivity of free space $= 8.85 \times 10^{-14}$ F/cm, A the cross-sectional area of the sample, l the sample thickness, and $i = \sqrt{-1}$. The real part of the dielectric permittivity (ε') as a function of temperature (T) for $FeTaO_4$ and $CrTaO_4$ is shown in Fig. 5. The corresponding dielectric data for $MTiM'O_6$ oxides are shown in Figs. 6–10 for $FeTiNbO_6$, $FeTiSbO_6$, $CrTiNbO_6$, $GaTiNbO_6$ and $GaTiTaO_6$, respectively. Typical dielectric loss curves are also given for $FeTiNbO_6$ and $FeTiSbO_6$ and $CrTiNbO_6$ in Fig. 11.

In normal dielectrics, the permittivity increases with temperature monotonically while in ferroelectrics a sharp peak is observed at the transition temperature. However, in the case of relaxor ferroelectrics a broad peak in the permittivity vs. temperature plot, with large frequency dispersion is observed [23]. This broad anomaly known as a diffuse phase transition is believed to occur due to the dynamics of the polar nano-domains in the relaxor material. This anomaly is also seen in the temperature dependence of the dielectric loss (imaginary part of dielectric constant). The temperature T_m corresponding to the permittivity maximum shows a frequency-dependence that follows the Vogel–Fulcher behavior [24]

$$f = f_0 \exp(-E/k_B(T_m - T_{VF})) \quad (2)$$

where f_0 is a pre-exponential factor, E the barrier energy, k_B the Boltzmann constant, and T_{VF} is the Vogel–Fulcher temperature. This is characteristic of relaxor ferroelectrics. Another characteristic feature of relaxor ferroelectrics is the deviation from the Curie–Weiss law [25]:

$$1/\varepsilon' = \frac{T - T_c}{C} \quad (3)$$

where C is a constant and T_c is the transition temperature.

From the results, we make the following general observations. (i) Both the $MM'O_4$ oxides, $FeTaO_4$ and $CrTaO_4$, show normal dielectric behavior, unlike the corresponding Ti-containing analogs,

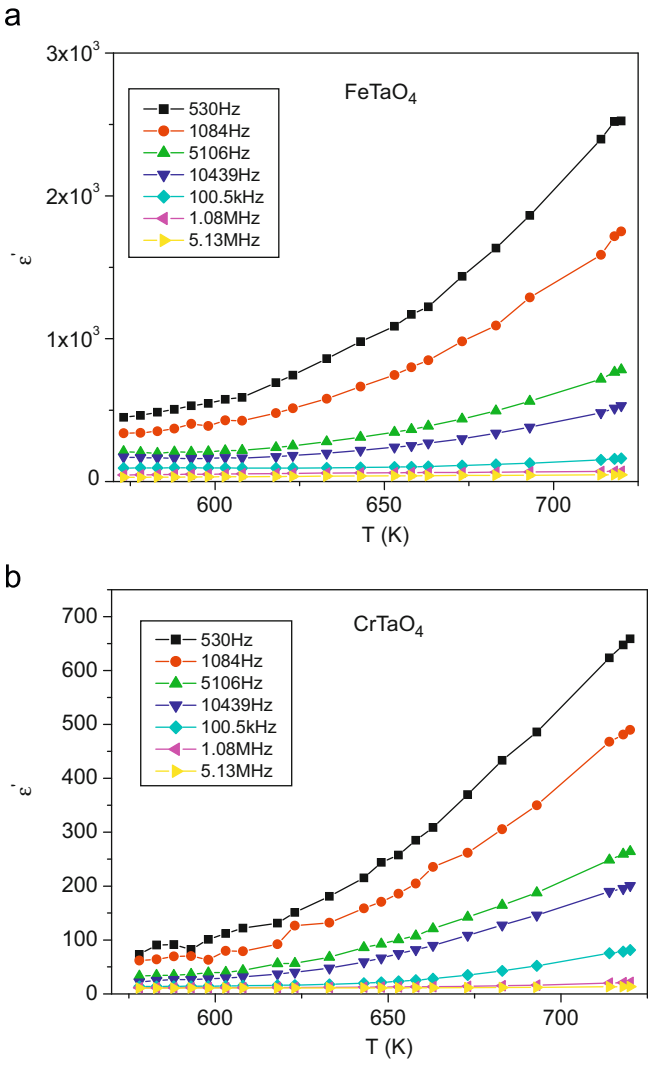

Fig. 5. Real part of the dielectric permittivity (ε') as a function of temperature at several frequencies for (a) $FeTaO_4$ and (b) $CrTaO_4$. In Figs. 5–10 solid lines connecting the data points are guides to the eye.

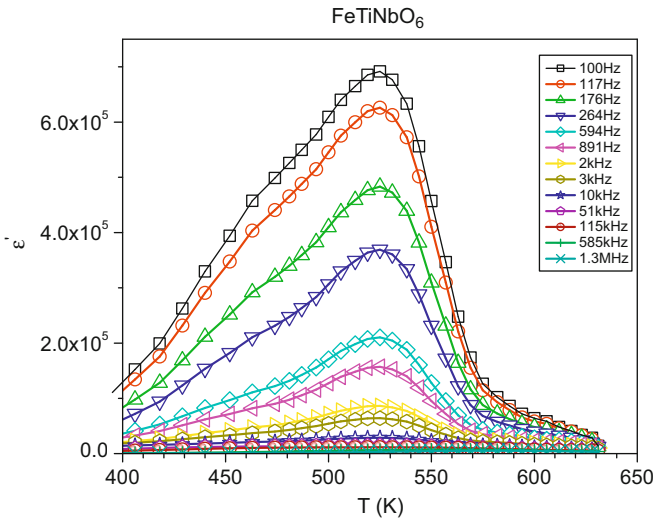

Fig. 6. Real part of the dielectric permittivity (ε') as a function of temperature at several frequencies for $FeTiNbO_6$.

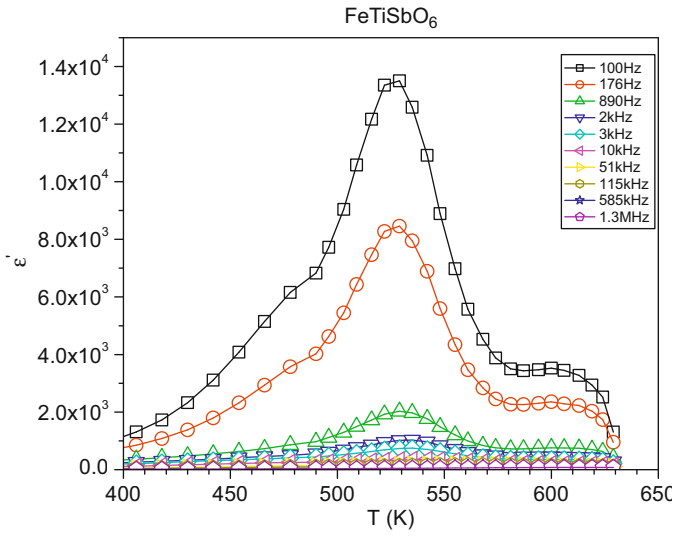

Fig. 7. Real part of the dielectric permittivity (ε') as a function of temperature at several frequencies for $FeTiSbO_6$.

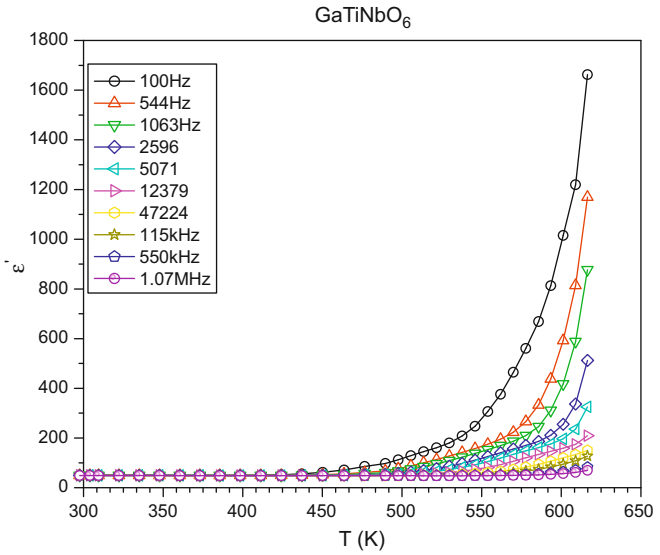

Fig. 9. Real part of the dielectric permittivity (ε') as a function of temperature at several frequencies for $GaTiNbO_6$.

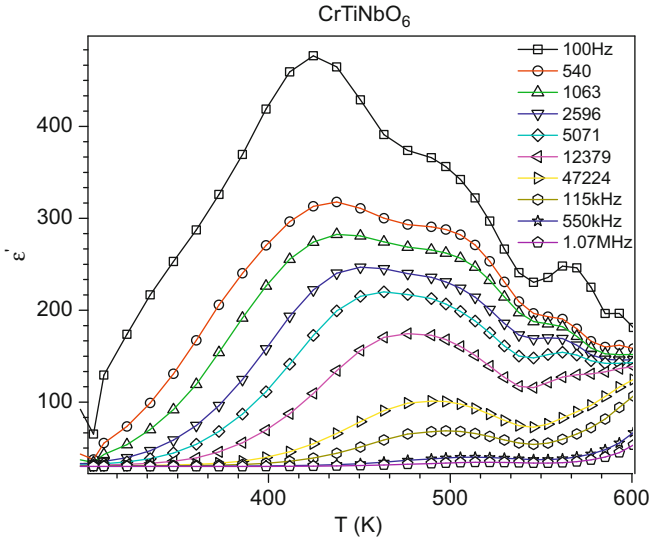

Fig. 8. Real part of the dielectric permittivity (ε') as a function of temperature at several frequencies for $CrTiNbO_6$.

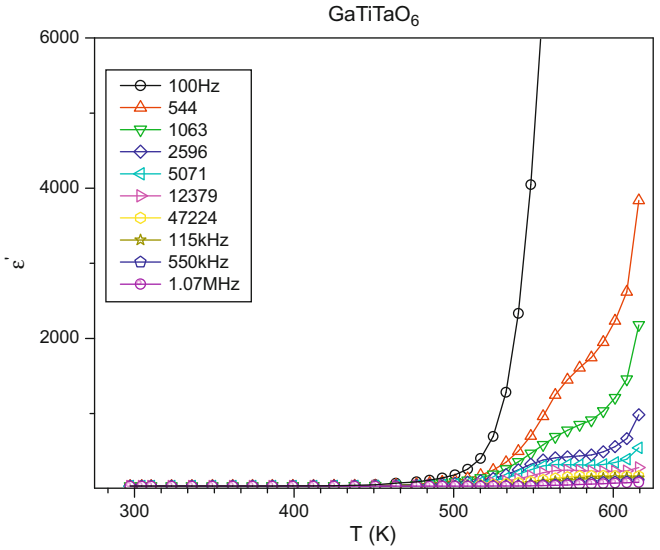

Fig. 10. Real part of the dielectric permittivity (ε') as a function of temperature at several frequencies for $GaTiTaO_6$.

$FeTiTaO_6$ and $CrTiTaO_6$, which show a relaxor ferroelectric behavior [5]. (ii) Among the $MTiM'O_6$ oxides investigated in this work, only those containing iron and titanium display a distinct relaxor/relaxor-like effect with giant dielectric constants that strongly depend on the frequency.

From the analysis of dielectric data {$1/\varepsilon'$ vs. T plot (Fig. 12) and Vogel–Fulcher fit (Fig. 13)}, we clearly see that $FeTiSbO_6$ shows a dielectric behavior that is characteristic of relaxors. On the other hand, a similar analysis of the data for $FeTiNbO_6$ showed a smaller frequency dispersion and a poor Vogel–Fulcher fit. Interestingly, the corresponding $CrTiNbO_6$ compound shows a typical relaxor dielectric response (Fig. 8), albeit with small dielectric constants. The latter however is comparable to that of $CrTiTaO_6$ [5]. (iii) In sharp contrast to the relaxor properties of $MTiM'O_6$ (M=Fe, Cr), we find that the corresponding gallium compounds, $GaTiNbO_6$ and $GaTiTaO_6$, do not show any relaxor-like response; instead, they exhibit (300–500 K) a normal dielectric behavior (Figs. 9 and 10).

We have also examined the a.c. electrical conductivity in the compounds showing relaxor-like response, i.e. $FeTiNbO_6$ and $FeTiSbO_6$ and $CrTiNbO_6$ (Fig. 14). The a.c. conductivity shows the typical frequency variation associated with ionic conduction. The somewhat large conductivity contribution in the Fe-based compounds makes it difficult to separate out the relaxations, and the large permittivity variation with frequency is possibly due to the defect-driven conductivity. However, the conductivity in the Cr-compound is rather small. From the loss curves (Fig. 11(c)), a true relaxor response in the case of $CrTiNbO_6$ is evident.

The present investigation therefore reveals that, for the occurrence of a relaxor-like response among the rutile oxides, the presence of titanium together with a transition metal (Fe/Cr) seems to be essential. A strong response is seen for Fe-containing oxides, although both $FeTaO_4$ and $CrTaO_4$ are not relaxors. Accordingly, titanium seems to be a crucial component for the occurrence of the

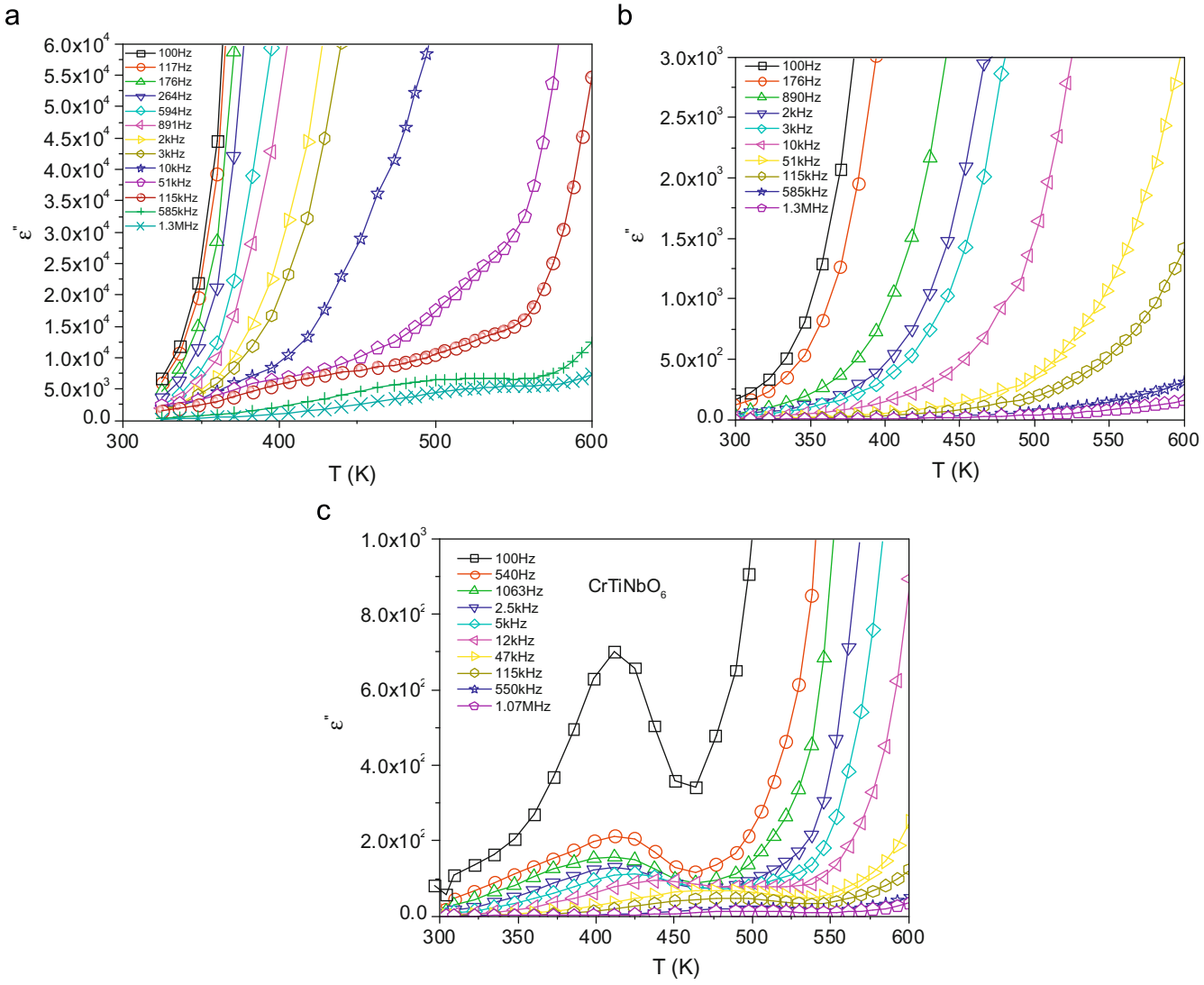

Fig. 11. Imaginary part of permittivity (dielectric loss) data for (a) $FeTiNbO_6$ (b) $FeTiSbO_6$ and (c) $CrTiNbO_6$.

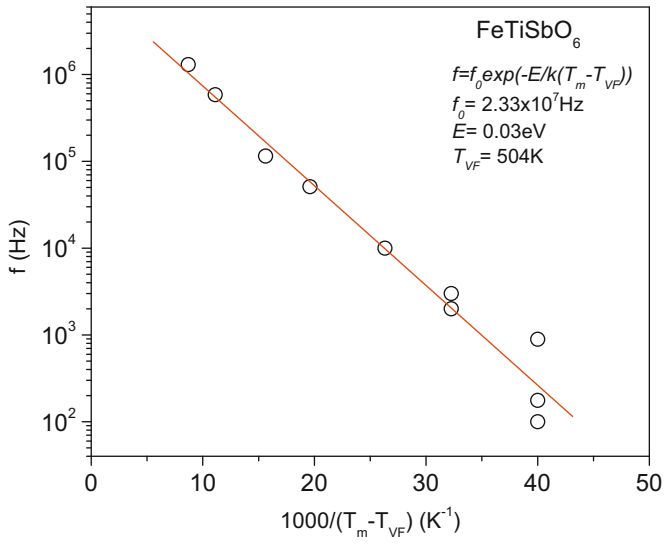

Fig. 12. Plot of inverse permittiviy ($1/\varepsilon'$) vs. temperature for $FeTiSbO_6$.

relaxor property. The observation of a relaxor-like response for $FeTiSbO_6$ suggests that Nb^V/Ta^V (d^0 configuration) does not appear to be crucial.

Structural [26] and theoretical [27] investigations of the incipient ferroelectric properties of rutile TiO_2 have indicated that an expanded rutile structure ('negative pressure effect') where the average Ti–O bond distance is larger than 1.960 Å would stabilize a ferroelectric response in the rutile structure. From our refinements of the structures of $MTiM'O_6$ oxides (Table 1), we find that in all the cases where there is a relaxor/relaxor-like response, the average M/Ti/M'–O distance is larger than that of rutile TiO_2, indicating a correlation between M–O bond lengths and relaxor-like response in these materials.

4. Conclusion

Our investigation of the dielectric properties of certain $MM'O_4$ and $MTiM'O_6$ (M=Fe, Cr, Ga; M'=Nb, Ta, Sb) rutile oxides have revealed the following systematics. (i) $MM'O_4$ oxides that do not contain titanium behave as normal dielectrics showing no relaxor

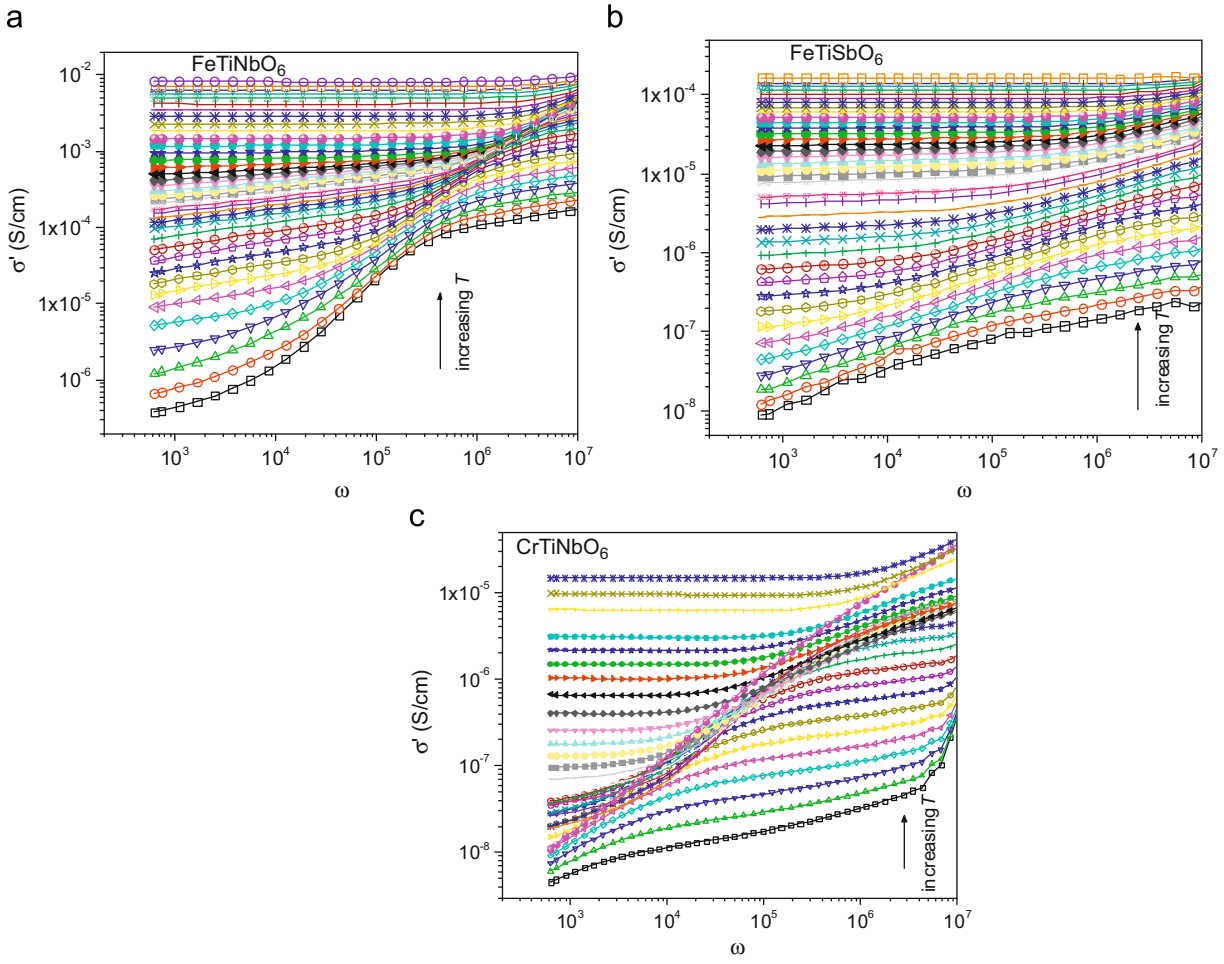

Fig. 13. Vogel–Fulcher fit of the dielectric maxima of $FeTiSbO_6$ for various frequencies and temperatures.

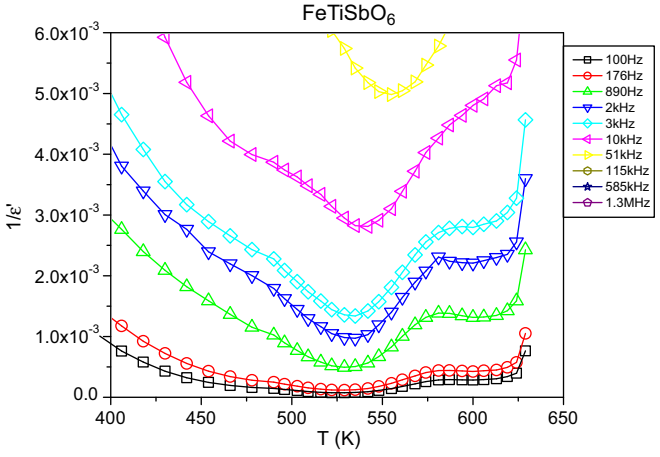

Fig. 14. Plot of a.c. electrical conductivity (real part) for (a) $FeTiNbO_6$ (b) $FeTiSbO_6$ and (c) $CrTiNbO_6$.

response. (ii) Among $MTiM'O_6$ oxides, those with M=Fe, Cr display a distinct relaxor effect, the response for iron being much stronger. (iii) The corresponding gallium analogs, $GaTiNbO_6$ and $GaTiTaO_6$, do not show a relaxor response. Oxides that show a strong relaxor effect contain titanium and a transition metal (iron or chromium) that seem to exert a 'negative pressure' resulting in the relaxor response, as predicted from theoretical investigation of pressure induced instabilities in bulk TiO_2 rutile structure [27].

Acknowledgment

J.G. thanks the Indian National Science Academy, New Delhi for the award of a Senior Scientist position.

Appendix A. Supplementary material

Supplementary data associated with this article can be found in the online version at doi:10.1016/j.jssc.2010.04.022.

References

[1] A. Fujishima, K. Honda, Nature (London) 238 (1972) 37.
[2] A. Mills, S. Le Hunte, J. Photochem. Photobiol. A 108 (1997) 1.
[3] C. Lee, P. Ghosez, X. Gonze, Phys. Rev. B 50 (1994) 13379.
[4] W.H. Baur, Crystallogr. Rev. 13 (2007) 65.
[5] R. Mani, S.N. Achary, K.R. Chakraborty, S.K. Deshpande, J.E. Joy, A. Nag, J. Gopalakrishnan, A.K. Tyagi, Adv. Mater. 20 (2008) 1348.
[6] L.E. Cross, Nature 432 (2004) 24.
[7] Y. Saito, H. Takao, T. Tani, T. Nonoyama, K. Takatori, T. Homma, T. Nagaya, M. Nakamura, Nature 432 (2004) 84.
[8] W. Lasocha, K. Lewinski, J. Appl. Crystallogr. 27 (1994) 437.
[9] W. Kraus, G. Nolze, J. Appl. Crystallogr. 29 (1996) 301.
[10] A.C. Larson, R.B. Von Dreele, General structural analysis system, Los Alamos National Laboratory, Report LAUR 86-748, 2000.

[11] J. Rodriguez-Carvajal, Fullprof 2000: A Program for Rietveld, Profile Matching and Integrated Intensity Refinements for X-ray and Neutron Data. Version 1.6, Laboratoire Leon Brillouin, Gif sur Yvette, France, 2000.
[12] Von M. Harder, H.k. Muller-Buschbaum, Z. Anorg. Allg. Chem. 466 (1979) 99.
[13] B. Morosin, A. Rosenzweig, Acta Crystallogr. 18 (1965) 874.
[14] G. Blasse, Mater. Res. Bull. 2 (1967) 497.
[15] A.N. Christensen, T. Johansson, B. Lebech, J. Phys. C: Solid State Phys. 9 (1976) 2601.
[16] W.H. Baur, W. Joswig, G. Pieper, D. Kassner, J. Solid State Chem. 99 (1992) 207.
[17] J.P. Doumerc, M. Vlasse, M. Pouchard, P. Hagenmuller, J. Solid State Chem. 14 (1975) 144.
[18] S. Siegel, H.R. Hoekstra, Acta Crystallogr. B 24 (1968) 967.
[19] V.H. Weitzel, S. Klein, Acta Crystallogr. A 30 (1974) 380.
[20] J.L. Forquet, A. Le Bail, P.A. Gillet, Mater. Res. Bull. 23 (1988) 1163.
[21] H. Weizel, Solid State Commun. 11 (1972) 313.
[22] D.C. Sinclair, A.R. West, J. Appl. Phys. 66 (1989) 3850.
[23] L.E. Cross, Ferroelectrics 76 (1987) 241.
[24] A.E. Glazounov, A.K. Tagantsev, Appl. Phys. Lett. 73 (1998) 856.
[25] D. Viehland, S.J. Jang, L.E. Cross, M. Wuttig, Phys. Rev. B 46 (1992) 8003.
[26] B. Jiang, J.M. Zuo, N. Jiang, M. O'Keeffe, J.C.H. Spence, Acta Crystallogr. A 59 (2003) 341.
[27] B. Montanari, N.M. Harrison, J. Phys.: Condens. Matter 16 (2004) 273.